Hindawi
Advances in Civil Engineering
Volume 2022, Article ID 1328583, 14 pages
https://doi.org/10.1155/2022/1328583

Research Article

Bending Performance of Precast Lightweight Aggregate Concrete Exterior Wallboard with a Concealed Rib Sandwich Structure

Congqi Li, Xinwei Ma, Ying Yang, Ahmed Ahmad Omar, Hao Wu, and Lei Qian

College of Civil Science and Engineering, Yangzhou University, Yangzhou 225127, China

Correspondence should be addressed to Congqi Li; licq@yzu.edu.cn

Received 19 November 2021; Revised 23 January 2022; Accepted 1 March 2022; Published 22 March 2022

Academic Editor: Li Chen

A new type of precast lightweight aggregate concrete exterior wallboard is proposed in this study. It is composed of inner and outer panels, an insulation layer, and concealed ribs. After adjusting the mixing ratio of lightweight aggregate concrete, light weight, bearing capacity, and good workability were guaranteed. The flexural performance of the composite exterior wallboard was studied by testing and numerical modeling of four wallboards, and the results of deflection, crack morphology, failure mode, and ultimate flexural capacity were then obtained. Additionally, the cracking and bending properties of the composite exterior wallboard were observed, and the calculation method of bending capacity and the cracking moment was studied. The calculated results coincided with the experimental data; therefore, this study provides a reference to the design and application of prefabricated exterior wallboards.

1. Introduction

Compared to traditional wallboard structures, the prefabricated exterior wallboard is characterized by excellent component quality, high construction efficiency, and green environmental protection [1], which is one of the important ways to change the wall and improve the level of building industrialization. As the building's peripheral protective components, the exterior wallboards should not only meet the mechanical properties but also the requirements of heat insulation, sound insulation, and waterproof of the protective structure.

Conventional types of exterior wallboards can be categorized as single material exterior wallboards, internal thermal insulation composite wallboards, exterior thermal insulation composite wallboards, and Sandwich thermal insulation composite wallboards. Among these, the Sandwich thermal insulation composite wallboard is composed of a concrete inner panel, insulation layer, and a concrete outer panel, where the inner and outer panels are often connected by rigid connectors. Compared with other forms of outer wallboard, the Sandwich thermal insulation composite wallboard has the advantages of thermal insulation and durability [2]. During transportation, storage, and service, precast wallboards are normally affected by the piled weight and out-of-plane loads of wind. Since the insulation layer of the Sandwich panels has low strength and large deformation [3], the out-of-plane load of the wallboard is mainly sustained by the inner and outer panels [4, 5]. The wallboard is casted layer by layer, but its cowork performance is poor, and the overall load-carrying capacity is relatively weak. Therefore, a concealed rib Sandwich structure is proposed in this study.

Arubaye et al. [6] conducted double-shear tests on four different types of fiber-reinforced polymer (FRP) connectors and six-point bending tests on eight full-size concrete Sandwich plates and established an elastic analysis method for calculating the connectors, providing a method for predicting the cracking and deformation of Sandwich plates. Daniel Ronald Joseph et al. [7] conducted four-point bending tests on four concrete Sandwich plates, which were connected by steel strand mesh connectors. The test results showed that mesh connectors made a high contribution to the composition of the Sandwich plate, and the flexural

bearing capacity of the Sandwich plate was greatly related to the thickness of the plate. The bending capacity of the Sandwich plate was improved. Cox et al. [8] developed a star connector using needle glass fiber composite material (GFRP) and carried out pull-out, double-shear, and whole-plate bending tests on the composite plate. The test results indicated that the combination degree of the Sandwich plate was less than 6.5% only when the star connector was set at the end of the Sandwich plate, and the combination degree was improved by setting additional connectors. Scholars have performed a lot of research on precast concrete Sandwich plate connectors, and most of these works focus on rod or plate discrete connectors or continuous connectors made of FRP grids. Although the purpose of improving the bearing capacity has been achieved in these works, the complex constructions of the plates are not conducive to large-scale promotion.

For the innovative wallboard proposed in this study, the inner and outer panels are made of fiber-reinforced lightweight aggregate concrete, and the insulation layer is made of polystyrene particle concrete. Using the same cementitious material is convenient for the preparation of wallboards. At the same time, steel trusses are set up between the inner and outer panels to form concealed ribs as shown in Figure 1. The rib structure is beneficial to improve both the mechanical performance of precast composite wallboards and the cooperative performance of inner and outer panels.

This study is organized as follows: in section preparation of lightweight aggregate concrete, bearing capacity and good workability are based on the main control index of density, compressive strength, and slump. Taking density, softening coefficient, and strength as the main control indexes, the polystyrene granule concrete of lightweight, waterproof, compact, and nondeformable is prepared. Subsequently, the out-of-plane static loading test [9] and numerical simulation of the mechanical properties of the concealed ribbed Sandwich outer wallboard are carried out in section establishment of the finite element model. The cracking condition, deformation performance, and bearing capacity of the wallboard are studied to observe the cooperative working condition and two-failure mode of the inner and outer panels under the loads outside of the plane that are included in section theoretical analysis to provide an extent of reference for the engineering application of the concealed ribbed Sandwich outer wallboard.

2. Materials and Methods

2.1. Mix Design. Optimum mix for lightweight aggregate concrete, five variables, gelled material, water-binder ratio, absolute volume sand ratio, mineral admixture content, and fiber content were used as design parameters. Through the single factor analysis method, the influence of five design parameters on compressive strength, dry density of the lightweight aggregate concrete was studied. All design parameters affect the slump of the mixture. In this study, the slump of the mixture was controlled in a reasonable range (80–100 mm) by adjusting the dosage of the water-reducing agent.

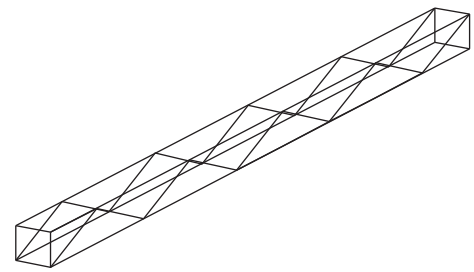

Figure 1: Schematic diagram of a concealed rib.

According to "The Technical Specification for Lightweight Aggregate Concrete (JGJ51-2002)" [10], the density grade of lightweight aggregate concrete prepared is 1,800 kg/m^3, the strength grade is LC30, and the slump is 80–100 mm.

Table 1 shows the optimal mixture ratio of lightweight aggregate concrete, with total cementitious material 460 kg, water-binder ratio 0.27, sand ratio 34%, fly ash 10%, slag 10%, and polypropylene fiber (PP fiber) content 0.05%.

Optimal mixture ratio of polystyrene granule concrete, the three variables of dispersible latex powder, hydroxypropyl methyl cellulose (HPMC), the gelled material, and the amount of lubricant are taken as the design parameters. The effects of three-design parameters on the viscosity, dry density, compressive strength, and softening coefficient of polystyrene granular concrete are studied by the single factor analysis. The optimal mixture ratio of polystyrene granular concrete is shown in Table 2 with water-binder ratio 0.5, PP fiber particle 30, gelled material 5.1 kg, fly ash 20%, zinc stearate 0.051 kg, redispersible latex powder 0.153 kg, and HPMC 3%.

2.2. Bendability Test of Precast Outer Wallboard. An out-of-plane static load test was carried out on the concealed rib Sandwich exterior wallboard [6] to study the influence of the thickness of the inner and outer panels, the setting of concealed ribs, the arrangement of concealed ribs on cracking and crack development, deformation performance, and bearing capacity of wallboard. The cooperative working condition and failure mode of the inner and outer panels under the exterior planeload were investigated. The results provide a reference for the engineering application of concealed ribbed Sandwich exterior wallboard.

2.3. Specimen Design and Manufacture. Considering the influence factors such as the thickness of inner and outer panels, whether the concealed rib is set or not and the way of arrangement, four groups of specimens were designed to carry out the static load test of the Sandwich wallboard under out-of-plane load.

The test simulation object is the prefabricated whole plate, that is, the height of the board is the height of the floor and the width of the plate is the size of the building space. Restricted by the test loading conditions, the specimen adopted the 1/2 scale, the size of the four test plates was 1600 mm × 1400 mm, and the total thickness of the wall plate was 130 mm. The inner and outer plates had an equal

Table 1: The optimal mixture ratio of lightweight aggregate concrete.

Cement (kg)	Slag: fly ash (%:%)	Slag (kg)	Fly ash (kg)	Sand (kg)	Ceramsite (kg)	Water (kg)	PP fiber (%)	Water reducing agent (%)	Sand ratio (%)	Binder (kg)	Water-binder ratio (%)	Slump (mm)
368	10 : 10	46	46	640	365	124	0.05	1.60	34	460	0.27	90

Table 2: Mixture ratio of polystyrene granule concrete.

Water-binder ratio	PP particle /L	Fly ash (kg/m^3)	Water (kg/m^3)	Cement (kg/m^3)	Zinc stearate (kg/m^3)	Redispersible latex powder (kg/m^3)	Gelled material (kg/m^3)	PP fiber (%)	HPMC (%)	Water-binder ratio (%)	Retarder (%)
0.5	30	1.02	2.55	4.08	0.051	0.153	5.1	0.05	3	1.5	0.05

thickness of 40, 50 mm, and the insulation layer had a thickness of 30, 50 mm.

The inner and outer panels of the wallboards were made of fiber-reinforced lightweight aggregate concrete, and the proportion is shown in Table 1. The insulation Sandwich layer was made of polystyrene granule concrete, and the mixture ratio of polystyrene granule concrete is shown in Table 2. The basic parameters of Slab 1~Slab 4 are shown in Table 3. The inner and outer panels were reinforced with steel mesh. In Slab 3 and Slab 4, the concealed ribs were welded with the steel mesh in the vertical and both in vertical and horizontal directions. The horizontal section of the test wallboard is shown in Figure 2.

The wallboards were placed in layers in the order of inner panels, insulation layers, and outer panels. The time interval of each layer was less than the initial setting time of concrete. The inner and outer panels of lightweight aggregate concrete and polystyrene particle insulation layer were made of the same cementitious material, and the bonding force between each layer of wallboards was better.

2.4. Test Loading Device and Scheme. The four sides of the prefabricated wallboard are flexibly connected with the frame beam and frame column. Under the load outside the surface, the frame beam and frame column can only be regarded as the support of the wallboard. To facilitate loading, the test pieces were laid flat, simply supported on four sides, and vertically loaded. Most of the outside planeloads, such as stacking load of prefabricated parts generated during transportation and installation and wind load during service, are uniform loads. In the test, the concentrated loading force was evenly distributed to the four loading points using a two-layer distribution beam, and the steel pads were also laid under the four loading points to simulate the plate loading [11]. The load testing device is shown in Figures 3 and 4.

The vertical displacement at the corresponding place of the top and bottom of the wallboards, the strain of reinforcement and concrete, and the occurrence and development of cracks were measured during the test. TAT3828E (signal test and analysis system) was used to collect electrical signals. The layout of the displacement meter, concrete strain gauge, and reinforcement strain gauge are shown in Figures 5, 6 and 7.

A load-controlled monotonic loading protocol is used according to the "Standard for Test Methods of Concrete Structures" [12]. The load is loaded at 5 kN per level, and the load lasts for 5 minutes. When the load reaches about 70% of the ultimate load, the load level of each level is adjusted to 10 kN/level until the load reaches the ultimate bearing capacity of wall panel members. When one of the following three conditions occur (i.e., the steel bar at the bottom of the wallboard specimen yielding or breaking, the upper concrete of the wallboard specimen crushing in the compression zone, and the crack width of wallboard or deflection exceeding an allowable value), the wallboard is considered to reach the bearing capacity limit state and the loading test ends.

3. Results and Discussion

3.1. Experimental Phenomena and Failure Modes. Under the action of monotone loading, the stress process of the specimen can be divided into three stages: cracking stage, yield stage, and limit stage. Figure 8 shows the crack distribution at the bottom and top of the Slab 1-Slab 4 wallboard.

3.1.1. Cracking Stage. At the beginning of loading, the first crack appeared in the bottom span, but the overall stiffness was good. The increase in inner and outer panel thickness and the setting of concealed ribs were beneficial to increase the cracking load of wallboards. The deformation characteristics of specimens before cracking were similar.

3.1.2. Yield Stage. With the increase in load, transverse cracks appear along the edge of the wallboard. The bonding interface between the inner and outer panels and the middle insulation layer was torn, the insulation layer began to compress, the integrity of the test plate became poor, and the stiffness rapidly decreased. The top of the wallboard gradually developed into annular cracks, the cracks at the bottom of the plate began to extend, and the reinforcement under the loading point at the bottom of the plate gradually yielded. There was no significant difference in fracture

Table 3: Test board basic parameters.

Number	Thickness of each layer of wallboard Outer panel: insulation layer: inner panel/mm	Concealed rib arrangement	Reinforcement ratio of inner and outer panels (horizontal/vertical)
Slab 1	40 : 50 : 40	0	0.559%/0.534%
Slab 2	50 : 30 : 50	0	0.559%/0.534%
Slab 3	50 : 30 : 50	Vertical	0.559%/0.577%
Slab 4	50 : 30 : 50	Horizontal/vertical	0.559%/0.577%

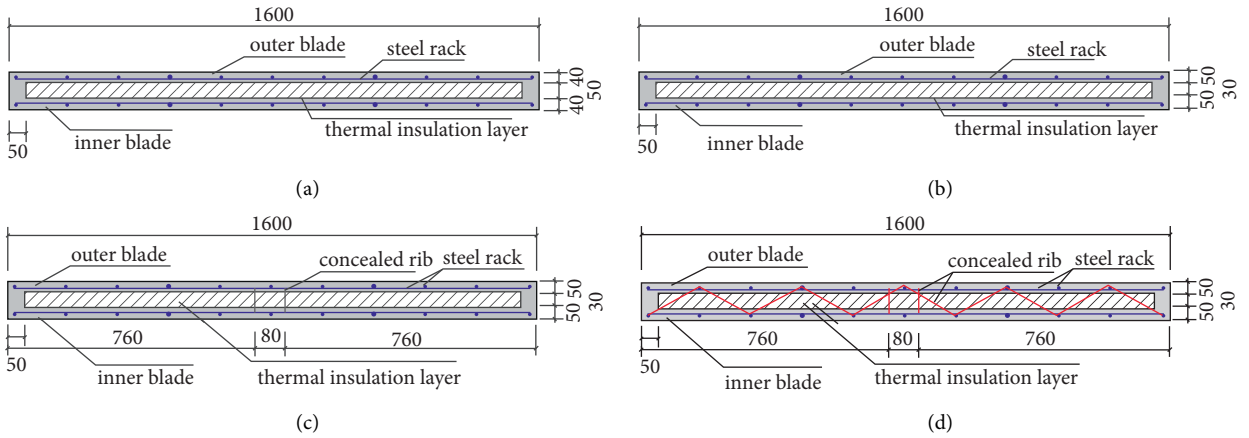

Figure 2: Horizontal section of wallboard: (a) Slab 1; (b) Slab 2; (c) Slab 3; (d) Slab 4.

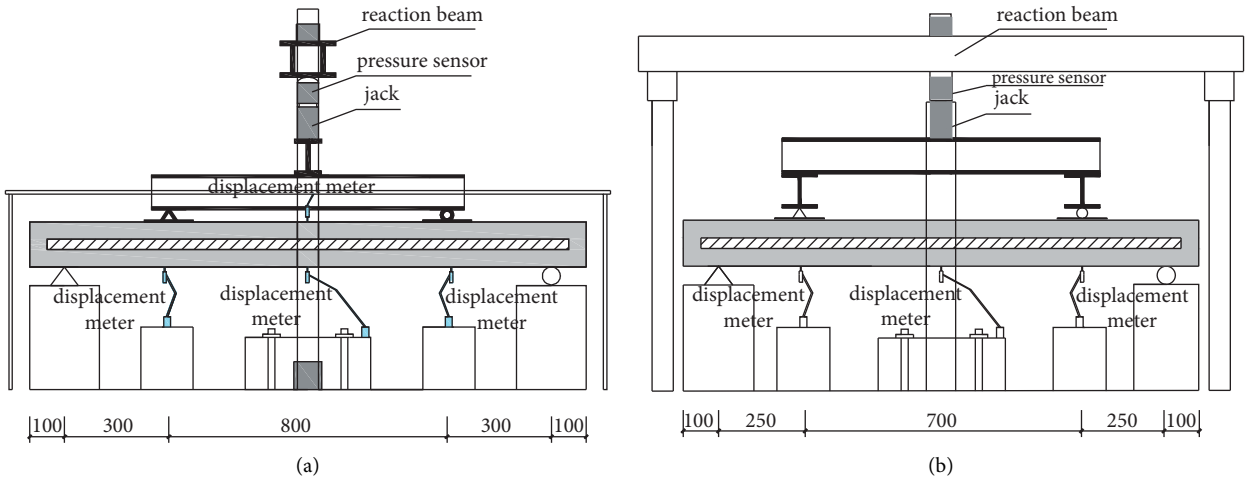

Figure 3: Schematic diagram of the test device: (a) the front view; (b) the side view.

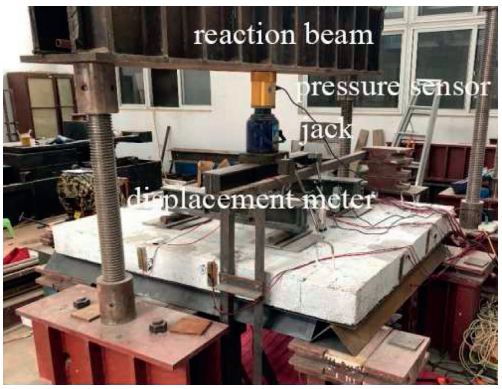

Figure 4: Field diagram of test loading.

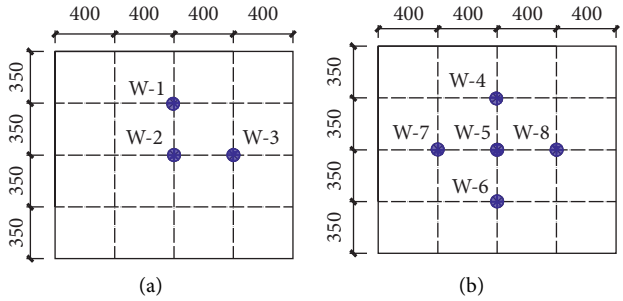

Figure 5: Layout of displacement meter: (a) top of the slab; (b) bottom of the slab.

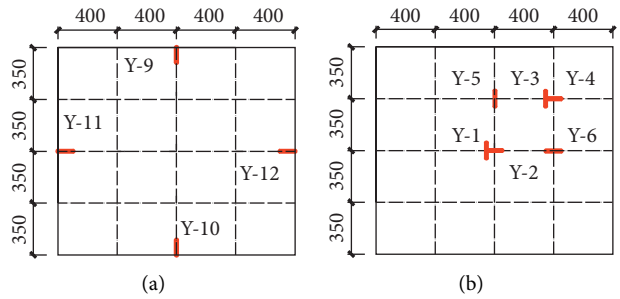

Figure 6: Layout of concrete strain gauge: (a) top of the slab; (b) bottom of the slab.

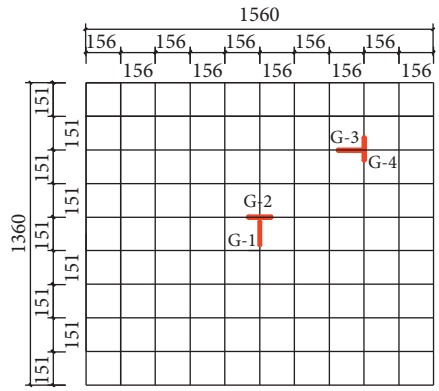

Figure 7: Layout of reinforcement strain gauge.

development between Slab 1 and Slab 2. In Slab 3, cracks along the concealed ribs appeared in the layout area of the wallboard top. The steel bar near the loading point at the bottom of the Slab 4 plate yield and the cracks at the bottom extended to the sides of the plate. The experimental phenomenon showed that the rib divided the wallboard into several continuous panels and improved the overall stiffness of the wallboard.

3.1.3. Limit Stage. As the load increased, the insulation layer was crushed, and the bottom cracks were fully developed. This formed radial cracks along with the four loading points, and oval circular cracks formed at the top of the wallboard. The four loading points on the top of Slab 1 finally lost their bearing capacity and cracked due to insufficient local pressure. Cracks of Slab 2 were fully developed, and the loss of bearing capacity was due to the yield of steel bars in the bottom span. The ultimate load of Slab 3 increased, the cracks at the bottom of the wallboard fully vertically developed along with the specimen, and the cracks at the top of the plate appeared in a circular closed direction parallel to the concealed rib. The concealed rib divided the specimen into two one-way plates, but it was deformed by the vertical load and could only be used as weak support. In Slab 4, the vertical and horizontal concealed ribs transferred part of the load to the edge of the test plate. Cracks at the bottom of the plate were few, but the development form was similar to that of other plates. The loss of bearing capacity was due to the yield of steel bars at the bottom of the plate.

3.2. Load-Deflection Curve. The deflection characteristic values of the test plate are shown in Table 4. The mid-span load-deflection curve of the plate bottom span is shown in

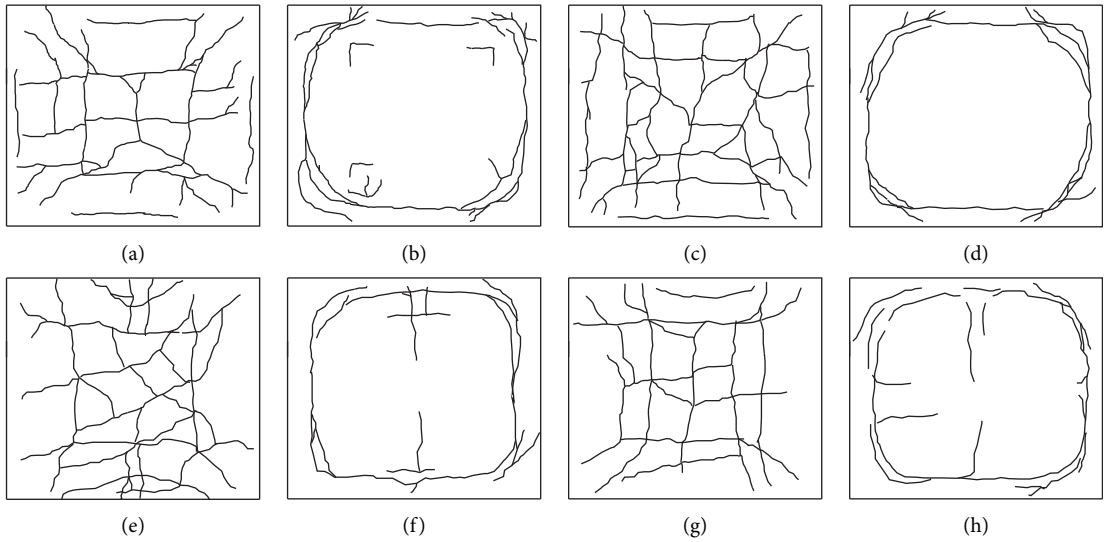

Figure 8: Cracks development diagram in the top of and at bottom of Slab 1–Slab 4: (a) bottom of Slab 1; (b) top of Slab 1; (c) bottom of Slab 2; (d) top of Slab 2; (e) bottom of Slab 3; (f) top of Slab 3; (g) bottom of Slab 4; (h) top of Slab 4.

Table 4: Eigenvalue of deflection of the specimen.

Number	Δcr (mm)	Δy (mm)	Δu (mm)
Slab 1	0.84	3.54	13.43
Slab 2	0.89	3.56	13.45
Slab 3	0.60	2.57	10.96
Slab 4	0.49	2.53	10.75

Note. Δcr is the cracking deflection, mm; Δy is the yield deflection, mm; Δu is the ultimate deflection, mm.

Figure 9. Figure 10 shows the comparison of top and bottom deflections of each wallboard at the same position.

Considering Table 4 and Figure 9, it can be seen that (1) the load-displacement curves of Slab 1 and Slab 2 before yield loading are similar in shape, and both show linear changes. The increase in the inner and outer panel thickness improves the stiffness of wallboards. When the yield load is reached, the wallboard's stiffness decreases, the increased rate of wallboard deflection exceeds that of the load, and the load slowly increases, but the increase in the inner and outer panel's thickness to the wallboard stiffness still takes place. (2) The overall stiffness of the wallboard of Slab 2 and Slab 3 is significantly improved by setting a concealed rib. After reaching the yield load, Slab 3 can still bear the slowly increasing load, and this indicates that the setting of the concealed rib can effectively improve the mechanical properties of the wallboard. (3) The load-displacement curve trend of Slab 3 and Slab 4 is equivalent before reaching the yield load. The increase in concealed ribs further improves the stiffness of wallboards, when the yield load is reached, and the slope of the Slab 4 curve very slowly declines, therefore indicating the addition of vertical and horizontal concealed ribs at the same time results in better mechanical performance of wallboards.

Figure 10 shows the load-deflection curves of the top and bottom of the test plate at the same position. It can be seen from the figure that when the load is small, the deflection of the top and bottom of the plate is the same, and the inner and outer panels are subjected to the same stress and deformation. With the increase in load, due to the compression deformation of the core layer material, the deflection of the top of the plate gradually exceeds the bottom of the plate, and the deformation of the inner and outer panels is no longer consistent, which is also the reason for the cracks on the top of the plate. The results show that increasing the thickness of the inner and outer panels or arranging the concealed ribs can lead to inconsistent deformation between the top and bottom, increase the cracking load on the top of the plate, and improve the cooperative performance of the inner and outer panels.

3.3. Characteristic Value of Bearing Capacity. The characteristic values of the bearing capacity of the test plate are shown in Table 5.

Table 5 shows the following:

(1) Cracking load: The increase in the inner and outer thickness of Slab 1 and Slab 2 can increase the cracking load by 58%, reaching 38 kN. Compared with Slab 2 and Slab 3, the cracking load can be increased by 39%, up to 53 kN. From Slab 3 and Slab 4, it is shown that the effect of setting the concealed ribs horizontally and vertically at the same time is better. If the concealed ribs are placed in one direction, the cracking load can be increased by another 15%, reaching 61 kN. With the increase in inner and outer panel thickness, the 8-effect section height of the wallboard participating in the bending work increases. The setting of concealed ribs is like adding trabecula in the plate, reducing the span of the plate and reducing the stress in the plate.

(2) Yield load: In this experiment, a strain gauge is installed on the stress reinforcement in the plate to monitor the stress change. The plate load

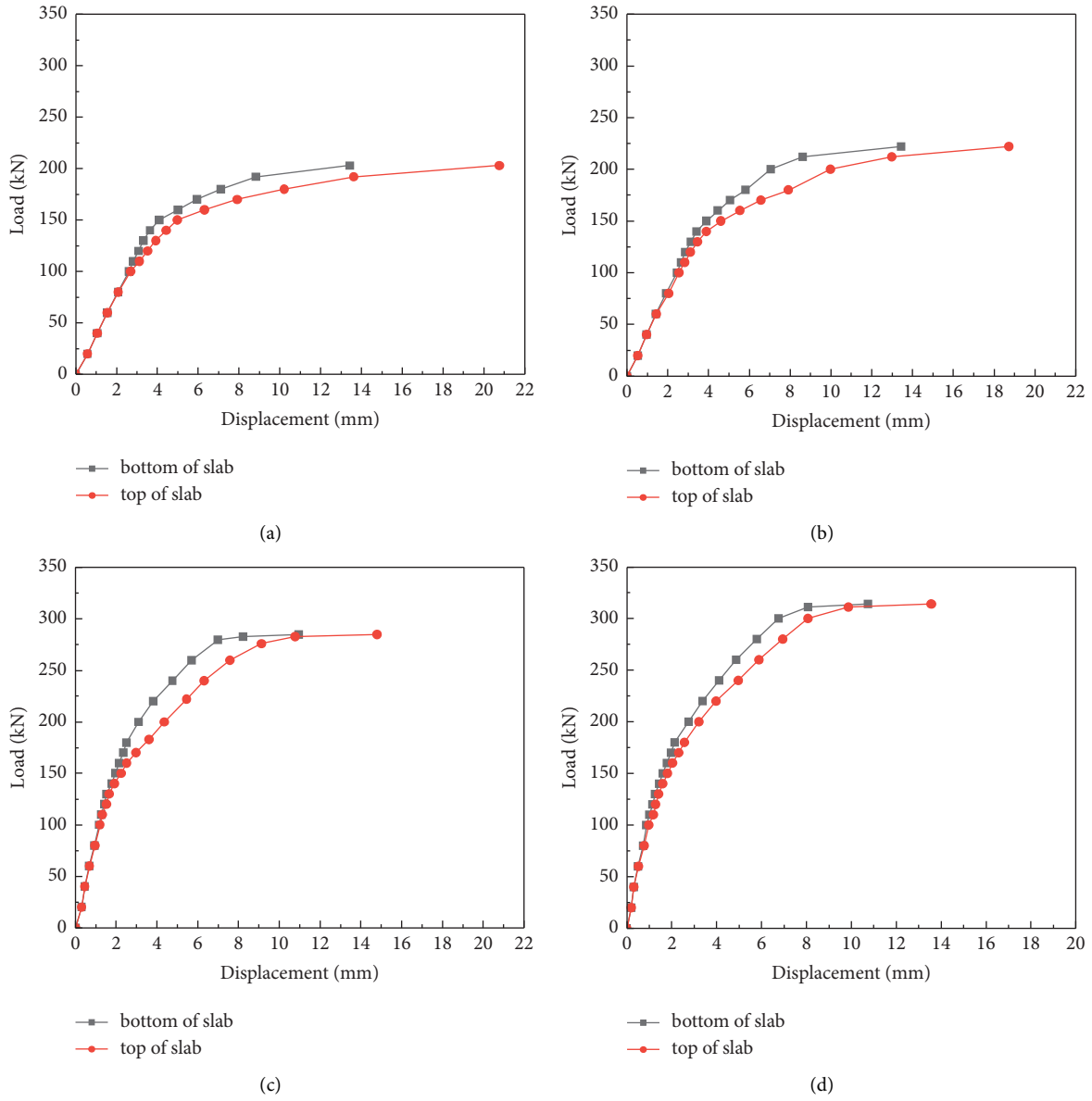

Figure 9: Load-deflection curves in the top and bottom of Slab 1-Slab 4: (a) Slab 1; (b) Slab 2; (c) Slab 3; (d) Slab 4.

corresponding to the stress reinforcement in the plate in the yield state is the yield load. The measured results of Slab 1 and Slab 2 show that the increase in inner and outer panels' thickness has little effect on yield load, only increasing by 4%, reaching 143 kN. Compared with Slab 2 and Slab 3, it is found that the setting of concealed rib causes the inner and outer panels to produce tension, restrict the mutual dislocation of the inner and outer panels, and can increase the yield load by 27%. Compared with Slab 3 and Slab 4, the setting concealed ribs in both vertical and horizontal directions in the middle of the wallboard can improve the yield load of the wallboard to a certain extent, but the effect is not significant, because it only increases by 10%.

(3) Ultimate load: Considering Slab 1 and Slab 2, the increase in inner and outer panels' thickness has little contribution to the ultimate bearing capacity, since it only increases by 10%. The Slab 3 test structure shows that the bearing capacity of the wallboard significantly increases after a concealed rib is installed, which is because the concealed rib forms a tie between the inner and outer panels of the wallboard, which effectively improves the cooperative performance of the inner and outer panels of the wallboard and improves the overall stiffness of the wallboard. In the loading process of Slab 1 and Slab 2 wallboards, when the load reaches 70% of the ultimate bearing capacity, the thermal insulation material of the core layer compresses and slips between the inner and outer panels. The interface between the inner

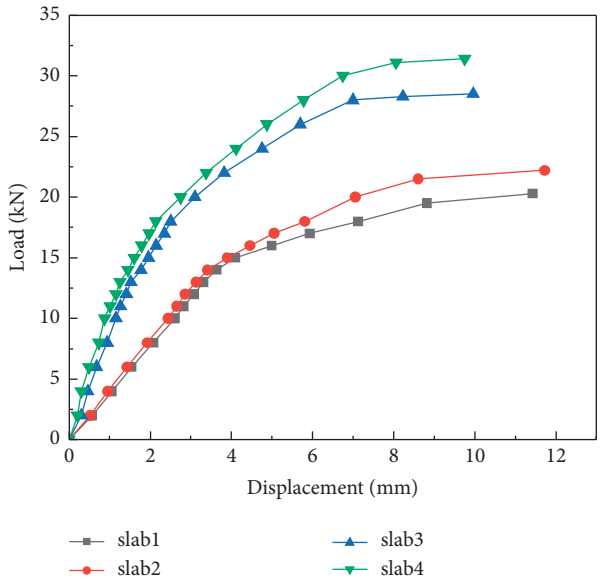

Figure 10: Load-deflection curves at the bottom of Slab 1–Slab 4 in the plate across.

Table 5: Characteristic value of bearing capacity of the test plate.

Number	*Fcr* (kN)	*Fy* (kN)	*Fu* (kN)
Slab 1	24	137	203
Slab 2	38	143	223
Slab 3	53	182	285
Slab 4	61	213	314

Note. *Fcr* is cracking load, kN; *Fy* is yield load, kN; *Fu* is the ultimate load, kN.

and outer panels and the thermal insulation layer of the core layer shifts, and the concealed rib can effectively contain the slip. When the load is more than 70% of the ultimate bearing capacity, this phenomenon was not present in Slab 3 and Slab 4 wallboards, and the bearing capacity of Slab 3 is 28% higher than that of Slab 2; however, a concealed rib is added and a plate stiffness of the out plane is improved. The wallboard channel bearing capacity increased by 10% when the concealed ribs are set in the vertical and horizontal direction, which is compared with that in one direction, and this is due to the fact that the concealed rib is like a trabecular, reducing panel plate across both inside and outside, makes the stress distribution more homogeneous in the plate, and improves the mechanical properties of plate, which indicates that concealed ribs could effectively improve the whole performance of the inner and outer panel and cause the wall stress more reasonable.

4. Numerical Simulation

Due to the limited test conditions, the numerical simulation of the flexural performance of prefabricated outer wallboards was carried out to provide a reliable numerical model for the later parameter analysis and further optimization of the plate shape.

4.1. Establishment of the Finite Element Model. ABAQUS finite element software was used to analyze the stress distribution and deformation of the composite wallboard under vertical load. During the modeling process, the concrete composite plate in Figure 11(a) and the steel grid frame and rigid gasket in Figure 11(b) were established, respectively. To simplify the finite element analysis, the bond-slip between the two types of concrete and reinforcement was ignored, and the reinforcement grid was set as a "built-in area" embedded into the whole. The two kinds of concrete and cushion blocks adopted the "C3D8R" type hexahedron element, and the reinforcement grid adopted the "B31" type linear beam element. The established finite element model is shown in Figure 11. The four ends of the finite element model of the composite plate are simply supported and were loaded on four points. To prevent stress concentration, four rigid plates were set on the four sides and four loading points of the composite plate, respectively, and the rigid plates were bound with the concrete surface by using the tie technology.

4.2. Finite Element Model Validation. The stress and deformation of the composite wallboard model after finite element solution are shown in Figure 12.

The top stress of the composite wallboard was distributed along with four loading points, the stress at the bottom of the loading point was the largest, the stress at the bottom of the plate was distributed along the four edges of the bottom of the plate, and the maximum stress was applied to the four edges of the test plate near the edge. The strain on the top of the plate corresponded to the stress, and the maximum strain was located around the four loading points. The strain at the bottom of the plate also formed a ring along the four edges of the plate.

It can be seen from Figure 12(a) that the strain at the circled part was large, which is consistent with the crushing of Slab 1 in the test. In Figure 12(c), the strain increased at

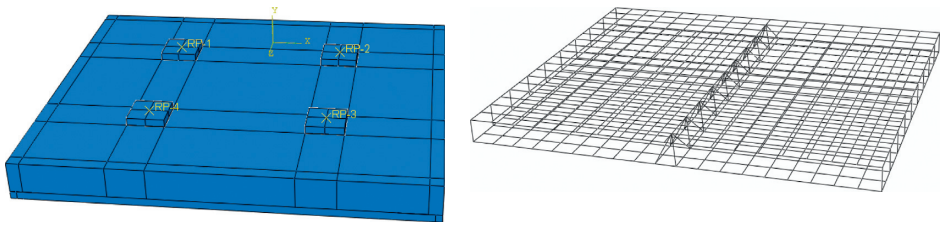

(a) (b)

Figure 11: Finite element structural model: (a) concrete panel; (b) steel rack.

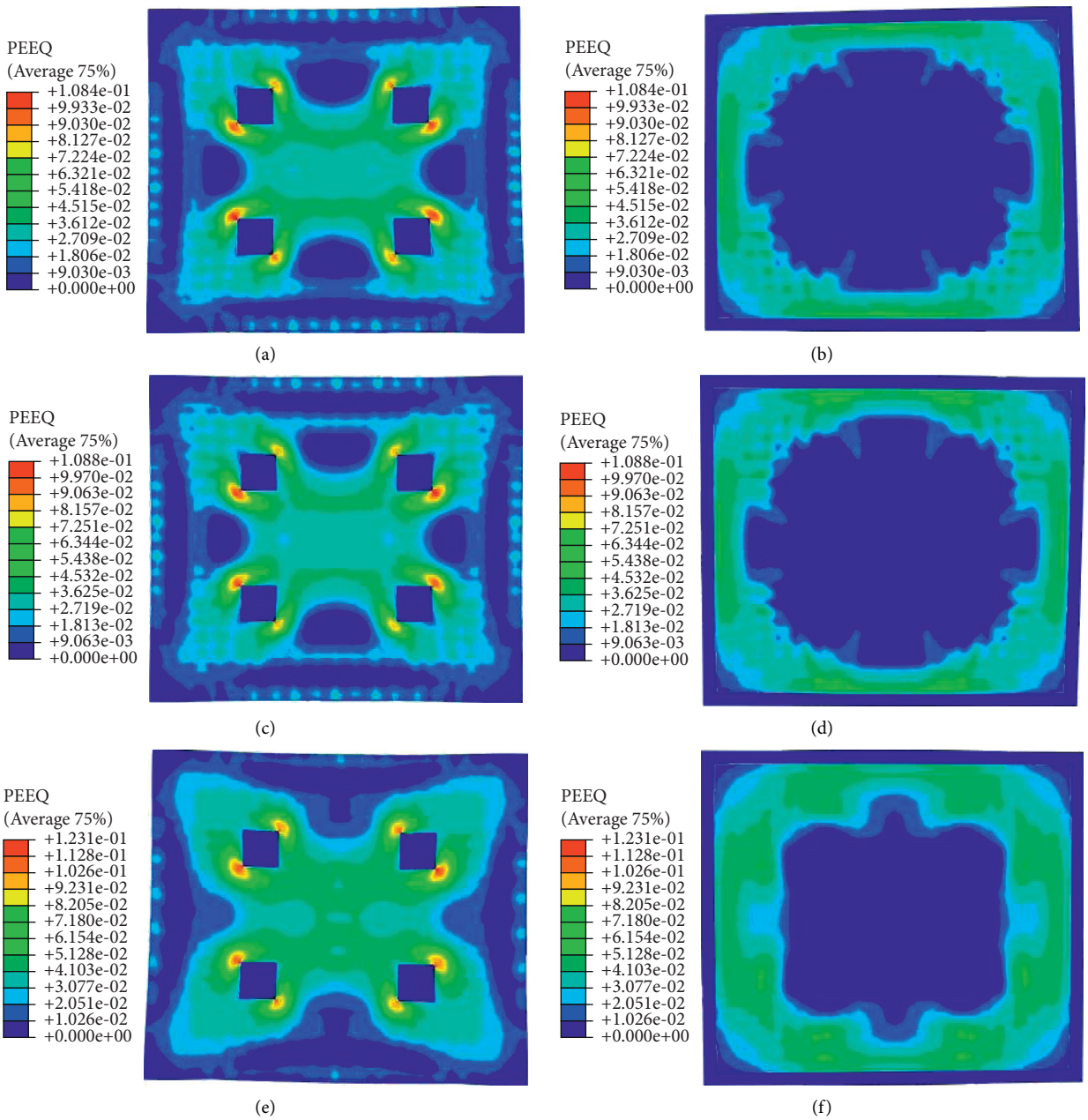

Figure 12: Continued.

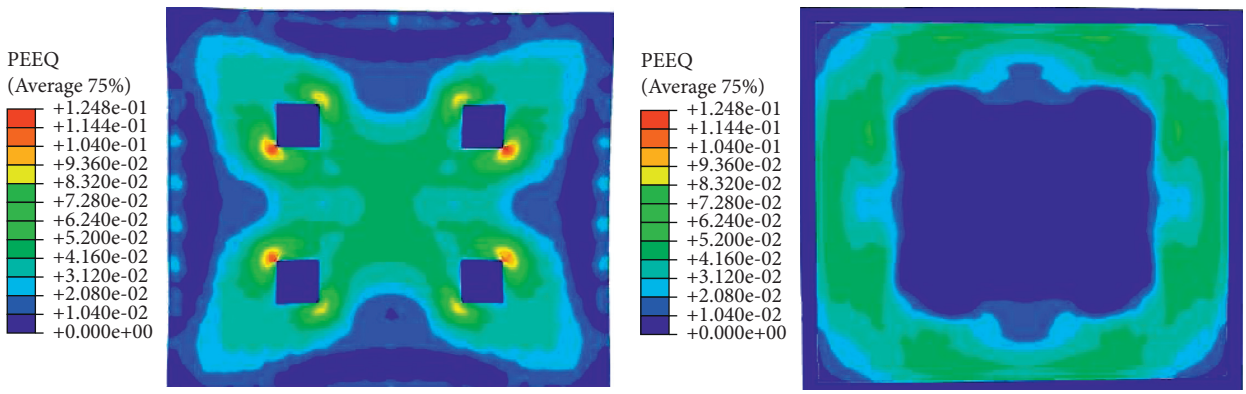

(g) (h)

Figure 12: Deformation cloud diagram of Slab 1–Slab 4 structural model: (a) top of Slab 1; (b) bottom of Slab 1; (c) top of Slab 2; (d) bottom of Slab 2; (e) top of Slab 3; (f) bottom of Slab 3; (g) top of Slab 4; (h) bottom of Slab 4.

the scribing part, corresponding to the annular crack at the top of the Slab 2 in the test. According to Figures 12(e), the line part was the layout area of the concealed rib, and the strain sharply increased on both sides of this area, which corresponded to the vertical crack along the concealed rib at the top of Slab 3 plate in the test. According to Figure 12(f), the strain at the bottom of Slab 3 corresponded to the strain on the top of Slab 3 and was also affected by the vertical concealed rib. According to Figures 12(g) and 12(h), the strain on both sides of the Slab 4 layout area with concealed ribs sharply increased, and the strain on the top and bottom of the plate was affected by the concealed ribs, which is consistent with the experimental failure phenomenon.

Figure 13 shows the comparison between the load-deflection curves of the mid-span of the structural model and curves of test results. The ultimate load obtained by test and finite element analysis is shown in Table 6.

As seen in Figure 13 and Table 6, the slope of the load simulation value is slightly larger than the test value of the load-displacement curve; however, the variation trend of the two values is the same. Slab 1 has the largest load value difference, and the test load is 88.6% of the simulated load. Slab 2 has the smallest load difference, and the test load is 96.1% of the simulated load. This indicates that ABAQUS finite element model can simulate the bearing capacity and deformation performance of the composite plate in a better way, and has good reliability in design and application. Other working conditions of this type of wallboard can be simulated by using the finite element model, which provides a basis for the shape optimization design of the composite wallboard.

5. Theoretical Analysis

5.1. Cracking Load of the Composite Wallboard. Concrete can be regarded as an elastic material due to its positive ratio of stress to strain before the composite wallboard reaches cracking load. When calculating the cracking load of composite wallboard with uniform material, the equivalent section can be obtained by converting the reinforced section to the concrete sectional area. Equivalent converted sections of composite wallboard before cracking are shown in Figures 14 and 15. When the cross-sectional area of bidirectional reinforcement is converted into concrete, an additional area is added at the upper and lower ends of concrete as $A_{sx'}$ and $A_{sy'}$, $A_{sx'} = A_{sx} \times n$, and $A_{sy'} = A_{sy} \times n$. Among them, A_{sx} represents the cross-sectional area of reinforcement in the X direction; A_{sy} represents the cross-sectional area of reinforcement in the y direction; $n = E_s/E_c$ represents the ratio of elastic modulus of reinforcement and concrete. The stress on the converted area of the reinforcement is equal to the strain force ($\varepsilon_s E_s$) of concrete at the corresponding section height.

5.2. Advice on Equations. According to the literature [13], the bending stiffness reduction coefficients in x and y directions are as follows:

$$\lambda_x = 1 - \frac{3}{16} \times 3.14 \times \frac{(d/h)^3}{1 + (t_w/d)},$$
$$\lambda_y = 1.036 - 0.784 \times \frac{(d/h)^3}{1 + 0.1333 \times (t_w/d)}. \quad (1)$$

Here, d is the height of the thermal insulation layer; t_w is the spacing of hollow circular tubes, because there is no round pipe in the composite plate, and the value here is 0.

According to the Code for Design of Concrete Structures [14], the formula for calculating cracking moment is as follows:

$$M_{\text{crx}} = \gamma_m \lambda_x W_0 f_t^0,$$
$$M_{\text{cry}} = \gamma_m \lambda_y W_0 f_t^0. \quad (2)$$

Here, γ_m is the basic value of the influence coefficient of section resistance of concrete member; W_0 is the cross-sectional resistance moment. For a bidirectional hollow plate, the resistance moment of section in both directions is equal to the stiffness reduction factor in that direction multiplied by the resistance moment of section in the corresponding solid section; f_t^0 is tensile strength.

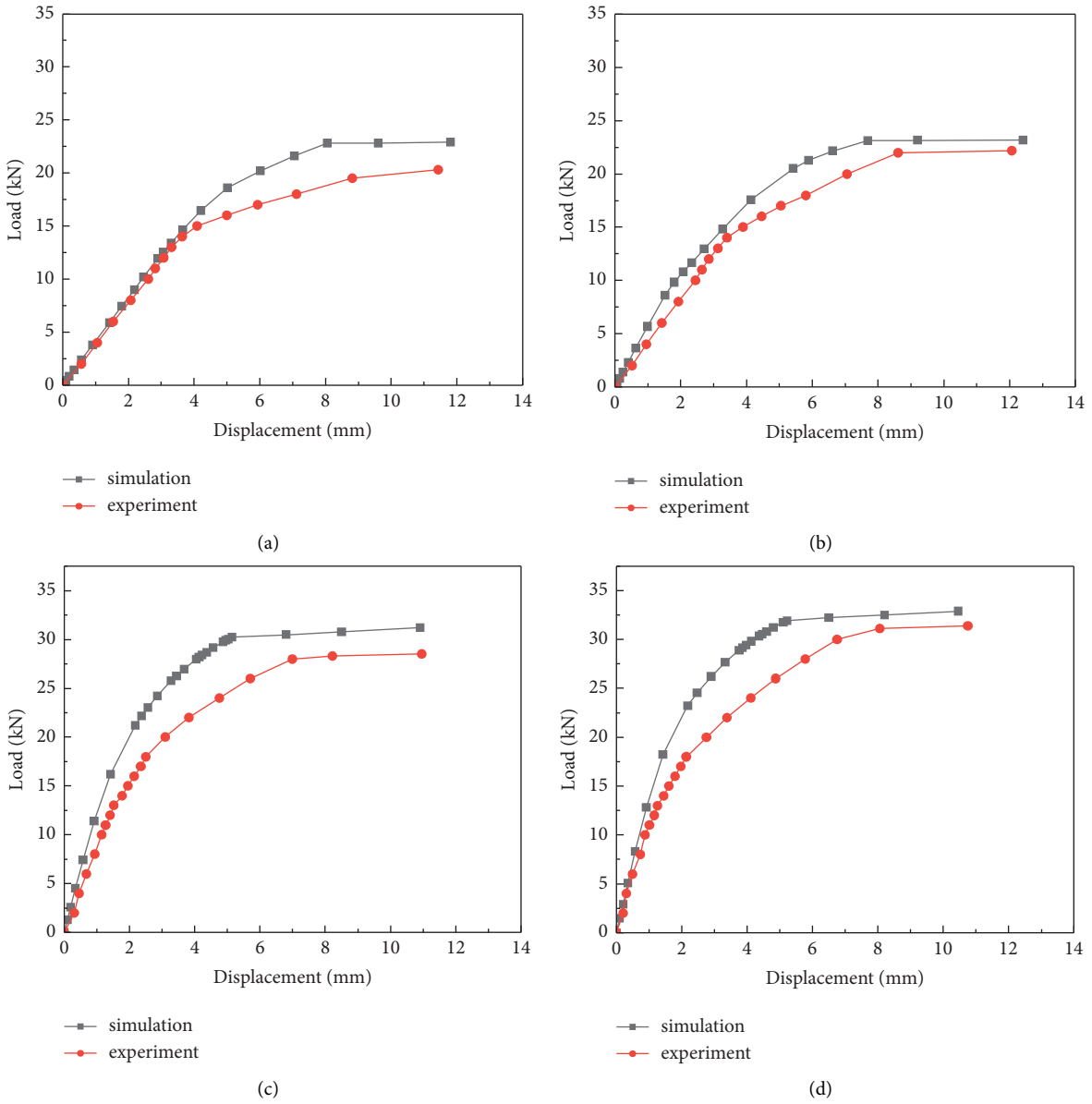

Figure 13: Comparison between simulated and experimental values: (a) Slab 1; (b) Slab 2; (c) Slab 3; (d) Slab 4.

Table 6: Comparison between simulated and experimental values of ultimate load.

Number	Simulated values (kN)	Experimental values (kN)	Error (%)
Slab 1	203	229	12.8
Slab 2	223	232	4.0
Slab 3	285	312	9.5
Slab 4	314	329	4.8
Average	—	—	7.8

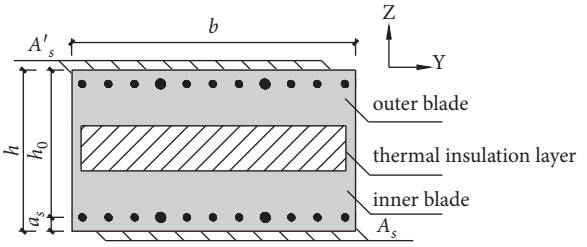

Figure 14: Schematic diagram of a normal section of the bidirectional plate.

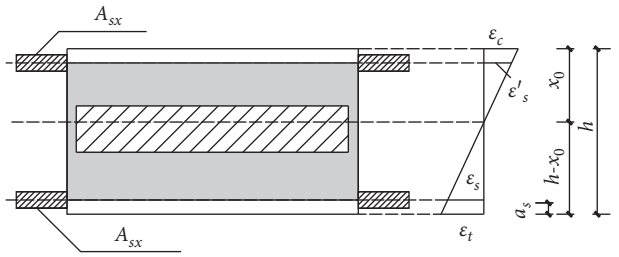

Figure 15: Equivalent converted section strain diagram.

The cracking load is as follows:

$$F_{\text{crx}} = \frac{M_{\text{crx}}}{l},$$
$$F_{\text{cry}} = \frac{M_{\text{cry}}}{l}. \tag{3}$$

The cracking load obtained from test and theoretical analysis is shown in Table 7.

It can be seen from Table 7 that the theoretically calculated value of the cracking load is generally close to the measured value of the test, with an average error of 12.8%, which can be used as the reference value in the test.

5.3. Composite Wallboard Bearing Capacity. The plastic stranding method is used to calculate the bearing capacity of four-side simply supported bidirectional dark ribbed composite wall slabs under uniform load. The longitudinal reinforcement direction span of the composite wallboard is l_x, the vertical longitudinal reinforcement direction span is l_y, and the included angle between the panel bottom oblique plastic hinge line and the long edge is θ. Reinforcement of the composite wallboard is equidistantly arranged, along the longitudinal reinforcement direction named x and vertical longitudinal reinforcement direction named y. The ultimate bending moment m_x and m_y within the width of the unit plate are as follows:

$$m_x = A_{sx} f_{sx} \gamma_{sx} h_{0x},$$
$$m_y = A_{sy} f_{sy} \gamma_{sy} h_{0y}. \tag{4}$$

Here, A_{sx}, A_{sy}, γ_{sx}, h_{0x}, and γ_{sy}, h_{0y} are the cross-sectional areas and internal couple arm of unit plate width in l_x and l_y directions, respectively. γ_{sx} and γ_{sy} are the coefficients of the internal moment arm and is usually taken as $\gamma_{sx} = \gamma_{sy} = 0.95$. f_{sx} and f_{sy} are the yield strength of the reinforcement in l_x and l_y directions, respectively.

According to the principle of virtual work, when the failure occurs under the action of the ultimate uniform load q, the virtual displacement at the midpoint of the plate is 1, and the virtual displacement at any point is $\omega(x, y)$. The work done by the exterior force (W_e) is equal to the work done by the internal force (the ultimate bending moment on the plastic hinge line) (W_i) [12, 15]. Then,

Table 7: Comparison of theoretical and experimental cracking load values.

Number	Calculated value (kN)	Experimental value (kN)	Error (%)
Slab 1	30	24	15.4
Slab 2	34	38	19.0
Slab 3	50	53	12.3
Slab 4	61	61	4.69
Average	—	—	12.8

$$W_e = q \sum_n \int\int_{A_n} \omega(x, y) dA_n,$$
$$= q\left[2 \times 2 \times \frac{1}{3} \times \frac{l_x}{2} \times s l_x + \frac{1}{2} \times l_x \times \left(l_y - 2s l_x\right)\right], \tag{5}$$
$$= \frac{q l_x}{6}\left(3 l_y - 2s l_x\right).$$

Here, A_n ($n = 1, 2, 3, 4$) is the area of each plate divided by the plastic hinge line.

When calculating the internal force work, let $l_y = n l_x$ and $m_y = \alpha m_x$; therefore,

$$W_i = -\sum m_i l_i \gamma_i,$$
$$= -\left(l_y m_x \cdot \frac{4}{l_x} + l_x m_y \cdot \frac{2}{x}\right), \tag{6}$$
$$= -2 m_x (2n + \alpha/s).$$

From $W_e + W_i = 0$, we can get the following:

$$q = \frac{2n + \alpha/s}{3n - 2s} \cdot \frac{12 m_x}{l_x l_y}. \tag{7}$$

According to the plasticity theory, the solution obtained by equation (7) is the upper bound. Therefore, the bearing capacity of the bidirectional composite slab should be all the solutions of equation (7).

The minimum value of the derivative of variable S can be obtained as follows:

$$\frac{\text{dq}}{\text{ds}} = \frac{(3n - 2s) - \alpha/s^2 + 2(2n + a/s)}{(3n - s)^2} = 0,$$
$$s = \frac{\alpha}{2n}\left(\sqrt{1 + \frac{3n^2}{\alpha}} - 1\right), \tag{8}$$
$$F = q \times A - G.$$

Here, G is the dead weight of the board.

The ultimate load obtained by theoretical analysis based on test and virtual work principle is shown in Table 8.

From Table 8, it can be seen that the theoretical calculated ultimate bearing capacity corresponds to the measured value in the test, with an average error of 6.6%. Therefore, it can be used as a reference value in the test.

Table 8: Comparison between theoretical and experimental values of ultimate load.

Number	Calculated value (kN)	Experimental value (kN)	Error (%)
Slab 1	230	203	13.3
Slab 2	231	223	3.6
Slab 3	282	285	1.0
Slab 4	288	314	8.3
Average	–	–	6.6

6. Conclusions

This study presents a type of precast concealed rib Sandwich outer wallboard. The wallboard is composed of lightweight aggregate concrete inner and outer panels, thermal core material, and concealed ribs between the inner and outer panels. The Sandwich structure of the wallboard allows it to have good thermal insulation performance. Meanwhile, the concealed ribs between the inner and outer panels effectively improve the mechanical performance of the wallboard. To fully optimize the Sandwich plate structure of the composite wallboard, the static load test, the finite element simulation, and the theoretical analysis are carried out. This is based on the inner and outer panel wall thickness and the arrangement of the concealed ribs on the Sandwich wallboard. Finally, the following conclusions are made:

(1) Comprehensive consideration of compressive strength, dry density, and workability. The optimal mixture ratio of LC30 lightweight aggregate concrete with excellent performance is obtained through test verification. The optimal mixing ratio is as follows: total cementitious material 460 kg, water-binder ratio 0.27, sand ratio 34%, fly ash 10%, slag 10%, and polypropylene fiber content 0.05%.

(2) By increasing the thickness of the inner and outer panels, the effective section of the wallboards participating in the bending work along the thickness direction is increased. Thus, the overall stiffness of the wallboards can be increased, which is conducive for improving the cracking load and ultimate bearing capacity of the wallboards, also improving the failure state of the wallboards.

(3) By setting concealed ribs between the inner and outer panels of the wallboard, the effective tie can be established, the cooperative performance of the inner and outer panels can be improved, and the overall stiffness, cracking load, and bearing capacity of the wallboard can be improved. At the same time, the relative dislocation slip between the inner and outer panels caused by the compression deformation of the core layer insulation material can be effectively alleviated. It is better to arrange the concealed ribs in both directions.

(4) The numerical model established can simulate the bearing capacity and deformation performance of the composite plate in a better way. The maximum value of bearing capacity obtained is close to the test value, which has good reliability and provides technical support for further optimization of the plate shape.

(5) The cracking load of composite wallboard calculated by the homogeneous elastic material method and the ultimate bearing capacity calculated by plastic stranding theory based on virtual work principle is close to the experimental value, which verifies the feasibility of this type of wallboard calculation method.

Data Availability

All data were obtained from own experiments. The test data are included in the article and can be made freely.

Conflicts of Interest

The authors declare that they have no conflicts of interest.

Acknowledgments

This research was supported by the Science and Technology Program of the Ministry of Housing and Urban-Rural Development, China (2020-K-114), the Construction System Science and Technology Project of Jiangsu, China (2018ZD096), and the Yangzhou Science and Technology Planning Project, China (YZ2020186).

References

[1] S. Zambelli and B. Zambelli, "Prefabricated concrete panel for industrialized building with high thermal and/or acoustic insulation," *Journal of the Acoustical Society of America*, vol. 116, no. 1, p. 1874, 2000.

[2] S. D. Zwanzig, *Numerical Simulation of Phase Change Material Composite Wallboard in a Multi-Layered Building Envelope*, University of Louisville, Kentucky, 2012.

[3] N. Lakshmanan, S. Ganapathi Chitra, J. Annie Peter, and R. I. Nagesh, "Behavior of light weight sandwich panels under out of plane bending loading," *Steel and Composite Structures: International Journal*, vol. 21, no. 4, pp. 775–789, 2016.

[4] P. L. N. Fernando, M. T. R. Jayasinghe, and C. Jayasinghe, "Structural feasibility of Expanded Polystyrene (EPS) based lightweight concrete sandwich wall panels," *Construction and Building Materials*, vol. 139, no. 15, pp. 45–51, 2017.

[5] L. Byoung-Jun and S. Pessiki, "Design and analysis of precast, prestressed concrete, three - wythe sandwich wall panels," *PCI Journal*, vol. 52, no. 4, pp. 70–83, 2007.

[6] S. Arubaye, T. Sorensen, J. Olsen, and M. Maguire, "Evaluating elastic behavior for partially composite precast concrete sandwich wall panels," *PCI Journal*, vol. 63, no. 5, pp. 71–88, 2018.

[7] J. Daniel Ronald Joseph, J. Prabakar, and P. Alagusundaramoorthy, "Experimental study on the flexural behavior of insulated concrete sandwich panels with wires as shear connectors," *Alexandria Engineering Journal*, vol. 58, no. 3, 2019.

[8] B. Cox, P. Syndergaard, S. Al-Rubaye, F. F. Pozo-Lora, R. Tawadrous, and M. Maguire, "Lumped GFRP star connector system for partial composite action in insulated precast

concrete sandwich panels," *Composite Structures*, vol. 229, Article ID 111465, 2019.

[9] G. Carbonari, S. H. P. Cavalaro, M. M. Cansario, and A. Aguado, "Flexural behaviour of light-weight sandwich panels composed by concrete and EPS," *Construction and Building Materials*, vol. 35, no. 5, pp. 792–799, 2012.

[10] China Academy of Building Research, *Technical Specification For Lightweight Aggregate Concrete, JGJ51-2002*, China Standard Press, Beijing, China, 2002.

[11] Standardization Administration of China, *Test Method for Building Wallboard, GB/T30100-2013*, China Standard Press, Beijing, China, 2013.

[12] Ministry of Housing and Urban-Rural Development, PRC, *Standard Test Method for concrete Structures, GB/T50152-2012*, China Standard Press, Beijing, China, 2012.

[13] X. Y. Han, S. G. Luan, and C. C. Wang, "Flexural stiffness analysis of cast-in-situ concrete hollow slab," *Industrial architecture*, vol. 39, no. S1, pp. 365–368, 2009.

[14] Ministry of Housing and Urban-Rural Development, PRC, *Code For Design of concrete Structures, GB50010-2010*, China Architecture and Building Press, Beijing, China, 2010.

[15] F. B. Wu, L. B. Deng, and B. Liu, "Experimental study on concrete composite floor slab simply supported by four sides with unidirectional pre-stressed and bidirectional reinforcement," *Building Structure*, vol. 44, no. 5, pp. 6–11, 2014.